International Journal of Hydrogen Energy 92 (2024) 1108–1120

Contents lists available at ScienceDirect

International Journal of Hydrogen Energy

journal homepage: www.elsevier.com/locate/he

Hybrid solar and hydrogen energy system 0-D model for off-grid sustainable power system: A case in Italy

Pier Paolo Brancaleoni, Giacomo Silvagni *, Vittorio Ravaglioli, Enrico Corti, Davide Moro

DIN – Department of Industrial Engineering, Alma Mater Studiorum – Università di Bologna, Bologna, 40121, Italy

ARTICLE INFO

Keywords:
Hydrogen power plant
Off-grid power plant
Control-oriented modelling
Italy case study
Sizing and modelling framework

ABSTRACT

Off-grid solar systems are one of the most promising solutions for achieving complete grid independence. However, the storage of large amounts of energy produced in the summer through solar panels becomes crucial to reach this goal and hydrogen, as a zero-CO2 energy carrier, could play a pivotal role. This paper presents a case study on the integration and simulation of solar energy and hydrogen technologies in an off-grid energy plant for a teaching buildings complex in Italy. A 0-D virtual energy plant model has been developed aimed at estimating the net energy production and hydrogen consumption/production rates using different inputs of irradiance (monthly average, daily) and energy demand (constant and variable daily consumption levels) in the buildings. The outcome of the analysis identifies the most convenient configuration of the plant in terms of sizing and device interactions for achieving complete grid independence, and the impact of different inputs on the plant performance.

1. Introduction

In recent years, the demand for energy has increased rapidly due to technological progress and population growth [1]. However, most of the energy is still produced from fossil fuels, owing to pollutants and Greenhouse Gases (GHG) emissions. In the European Union (EU) over 75 % of GHG emissions originate from the energy sector, prompting numerous measures to reduce these emissions [2]. Clean energy from renewable sources has emerged as a suitable solution for the reduction of GHG worldwide. According to the European Environment Agency, approximately 22.5% of energy in the EU is derived from renewable sources, with solar, wind, and hydro energy contributing the most [3]. The geographical position and morphology of a region significantly influence the production capacity of these renewable energy plants. The geographical position and the morphology of the territory strongly influence the production capacity of these plants. Italy, located in the centre of the Mediterranean Sea, is uniquely positioned for renewable energy production. In fact, renewable energy accounts up to 50% of Italy's total power production [4,5]. However, the intermittent availability of renewable energy (related to atmospheric and seasonal events) underlines the necessity for reliable energy storage systems to store excess energy when production exceeds demand [6]. While batteries are the most common solution for energy storage, their low specific energy capacity and reliance on critical materials increase the cost per stored watt-hour. Additionally, the carbon footprint of batteries is higher with respect to other alternative solutions, such as hydrogen, ammonia and methanation [7,8], which lead to consider battery packs not suitable for big energy storage. Numerous studies have highlighted the potential of hydrogen in decarbonizing the energy sector by bridging the gap between renewable energy production and energy demand. Marocco et al. [9] demonstrated that the optimal solution for off-grid power plants involves using both battery and hydrogen storage rather than oversizing the battery pack.

Hydrogen can be produced in different ways and with different energy sources [10,11]. Currently, Methane Steam Reforming (MSR) represents the most common process for hydrogen production (grey hydrogen); however, it results in significant GHG emissions due to heating processes usually performed with carbon-based fuels and side reactions [10]. To address these emissions, three main alternatives can be pursued. The first is based on carbon capture technologies which limit GHG emissions (blue hydrogen), although carbon-based fuels remain the primary energy sources [12]. On the other hand, water electrolysis offers a true carbon-free hydrogen production method, if energy used if from non-fossil sources. This leaves two viable options: nuclear energy (pink hydrogen) and solar/wind energy (green

* Corresponding author.
E-mail addresses: pier.brancaleoni2@unibo.it (P.P. Brancaleoni), giacomo.silvagni2@unibo.it (G. Silvagni), vittorio.ravaglioli2@unibo.it (V. Ravaglioli), enrico.corti2@unibo.it (E. Corti), davide.moro@unibo.it (D. Moro).

https://doi.org/10.1016/j.ijhydene.2024.10.284
Received 5 August 2024; Received in revised form 9 October 2024; Accepted 20 October 2024

Symbols/abbreviations

A_{PV}	Area of single PV
BP	Battery Pack
DOD	Depth of Discharge
E_{theo}	Theoretical energy produced by PVs
E_{nov}	Energy request in November
EU	European Union
FC	Fuel Cell
GHG	Greenhouse Gases Emissions
LHV	Lower Heating Value
MSR	Methane Steam Reforming
N	Number of PV
PV	Photovoltaic modules
SOC	State of Charge
SOH	State of Health
PEM	Polymer Electrolyte Membrane
P_{batt}	Power sent to battery pack
$P_{compressor}$	Power drain by compressor
$P_{electrolysis}$	Power available for electrolysis
P_{FC}	Power from FC
$P_{produced}$	Power produced by PV
P_{user}	Power sent to the user
β	Thermal losses
η_{BP}	Efficiency of BP
η_{FC}	Efficiency of Fuel Cell
$\eta_{Inverter}$	Efficiency of the Inverter
η_{PV}	PV Efficiency

hydrogen). Nuclear energy, however, is banned in several countries, including Italy, limiting its availability. Green hydrogen, produced using existing photovoltaic (PV) and wind power plants, enables the production of a CO2-free energy carrier. In this scenario, green hydrogen can be produced when the available energy from renewable sources is higher than the market request, stored, and then converted back to energy when needed. Although green hydrogen has the potential to reduce emissions, its adoption is currently limited by complexity and cost. However, its market share is anticipated to increase in the coming decades [13]. Among the possible electrolysis technologies, Polymer Electrolyte Membrane (PEM) electrolysers are notable for their high efficiency, hydrogen purity and low start-up times, making them suitable for these applications [14].

Once produced, hydrogen must be stored. In addition to challenges related to hydrogen production, effective storage systems are a major concern in developing a hydrogen-based infrastructure. In fact, molecular hydrogen is the smallest and least dense molecule in the universe in its gaseous form at ambient temperature and pressure. Therefore, specialized methods are required to store significant amounts of hydrogen in relatively small volumes. The most common method is gaseous compression, where storage pressures typically range between 100 and 1000 bar [15]. Standard electrolysers typically produce hydrogen at pressures between 2 and 20 bar, necessitating a dedicated compressor to achieve the desired storage pressure. Metal hydrides are another promising storage method [16–18], offering high reversible capacity, but their widespread application is limited by high costs. Even liquified hydrogen is a suitable storage method, however, cost and boil-off does limit its application in long-term applications [16,19].

In a conventional hydrogen-based energy system, stored hydrogen must be converted back into energy to meet increased energy demands. Several devices serve this purpose: hydrogen internal combustion engines [20], which convert chemical energy into mechanical energy and then electrical energy via an alternator; hydrogen burners, which directly burn hydrogen to obtain thermal energy [21,22], and Fuel Cell (FC) devices [23], where electrochemical reactions generate electric energy. FCs achieve higher conversion efficiencies compared to hydrogen fuelled internal combustion engine and perform optimally under steady-state operating conditions [24]. However, Battery Packs (BP) are usually integrated into hydrogen-based energy systems to manage fast transients in the energy demand [8].

Green hydrogen-based power plants are particularly compelling for off-grid applications where complete autonomy from the grid is necessary (i.e., remote locations or structures seeking independence from the grid). Many authors have highlighted the advantages related to the development and control of hydrogen-based off-grid energy systems [25–28]. To achieve complete autonomy from the grid without oversizing the plant, optimizing energy flow and developing dedicated control strategies are essential to minimize losses. Puranen et al. [28] studied the optimal design for off-grid power plant in northern climates, emphasizing the need to avoid high peak power demands to reach full independence from the grid: they concluded that neither pure battery storage nor pure hydrogen storage alone is sufficient to reach the goal. Guinot et al. [29] investigated the effect of aging in photovoltaic-battery-hydrogen hybrid off-grid power systems, suggesting that proper device management (e.g., limiting battery depth of discharge) can mitigate system aging over a 5-year period. Similarly, Babatunde et al. [30], focusing on the design of off-grid power system for African regions, concluded that hybrid solar-hydrogen-battery solutions are the most suitable for sustainable energy production in off-grid settings. Abdin et al. [31] analysed the impact of location (United States, Australia, and Canada) on components sizing for off-grid power plants, suggesting that a fully hydrogen-based energy system (i.e., without batteries) could potentially achieve complete energy independence, in the future. Ceylan et al. [32] estimated the payback period for hybrid solar-hydrogen power plants to range from 14 to 18 years, underscoring the importance of properly sizing the plant components.

This work presents a design framework for the sizing, modelling, and managing a solar-powered hydrogen-based power plant. A case study aimed at converting the primary energy source (electricity) of a teaching buildings complex in Italy will be presented. The layout of the plant and the size of the components have been defined based on energy need and availability based on daily energy management over the past years (2018–2021, excluded the 2020 since the consumption data could be altered by the COVID pandemic). The whole system has been modelled using a 0-D simulation environment to predict its performance and energy flow throughout a year at a 5 min resolution. Using this 0-D virtual power plant, to maximize overall efficiency and the State of Health (SOH) of the plant specifically designed control strategies have been developed. The proposed approach enables the design and testing of a hybrid solar-hydrogen off-grid power system, providing valuable insights into its expected performance over the course of a year.

2. Methods

This section details the design and modelling of the plant, as depicted schematically in Fig. 1.

The solar-hydrogen off-grid power system considered in this work consists of the following components: a photovoltaic array, BP, FC, electrolyser, high-pressure hydrogen compressor, and two reservoirs. The power generated by the PV is fed directly into the inverter providing energy for the buildings. The extra-power from the PV charges the battery pack through a booster (the PV array has lower output voltage with respect to the BP). If the power production exceeds demand and the battery is at full capacity, the extra power from PV is directed to the

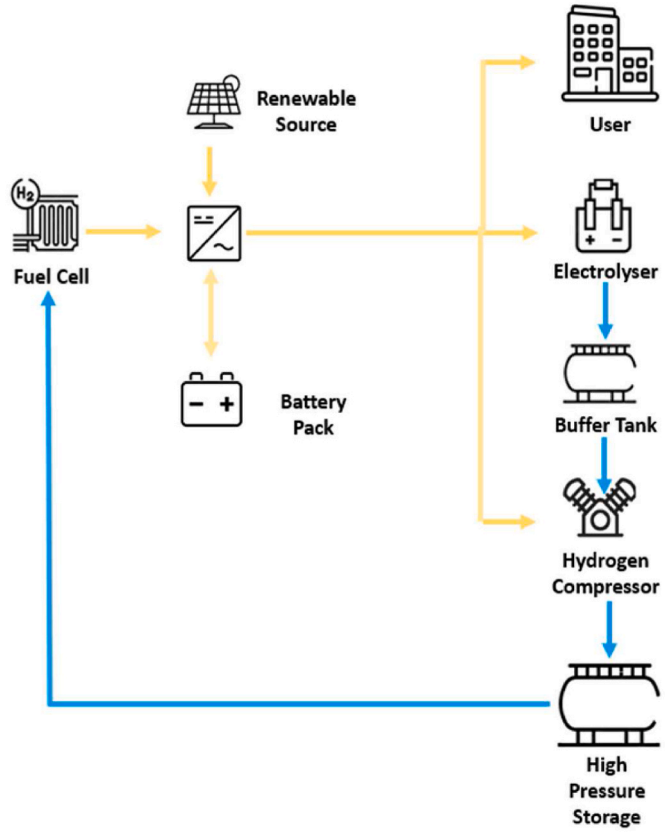

Fig. 1. Schematic representation of plant, energy flow (in yellow) and hydrogen path (in light blue). (For interpretation of the references to colour in this figure legend, the reader is referred to the Web version of this article.)

electrolyser, where hydrogen is produced and stored in a buffer tank. A volumetric compressor, connected to the inverter, increases the hydrogen's pressure and delivers it to the main high pressure storage tank. Finally, when the power from the PV is insufficient to meet user demand two scenarios can happen. If the battery is callable to deliver the requested power the battery is discharged, otherwise, the difference between the requested power and the available from the battery is provided converting back the hydrogen into energy through FC. Further considerations regarding energy flow and recharge strategies will be discussed in the next sections.

2.1. Components sizing

In this first subsection, the design of the plant is discussed, with particular focus on the sizing and selection of machines and components. Specifically, for these initial considerations, the plant is analysed considering actual monthly averages of energy demand and production.

The workflow for the sizing of the components is presented in Fig. 2.

2.1.1. Solar panel sizing

The first step of the sizing pathway consists in estimating the maximum number of photovoltaic modules and the corresponding theoretical energy production. The place this case study focuses on (Fig. 3) is the University Campus in Forlì, Italy, composed of six main buildings (latitude: 44° 219′, longitude: 12° 043').

As can be observed, some buildings have flat roofs, while other have sloped roofs. Considering the different roof slopes, the overall available area for PV was estimated. Table 1 summarizes the available surface per roof type.

The choice of the optimal inclination and orientation (azimuth angle) of the PVs depends on the geographical location of the site [33, 34]. The total irradiance (i.e., the total radiant flux per area that hits a surface) is influenced not only by the season and location, but also by the azimuth and inclination of the PV module [34]. For the sloped roofs, the azimuth and inclination of the PVs were set to match the inclination and orientation of the roof for ease of installation. For the flat roofs, the inclination was set to 0° to maximize the number of PV modules and avoid mutual shading between them. This configuration maximizes the total number of PVs, although the irradiance is below its maximum value. After calculating the available area and defining the orientation/inclination, the maximum number of PVs that can be installed

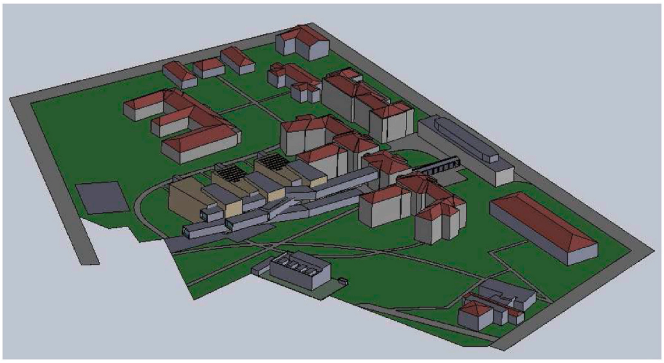

Fig. 3. Graphical representation of the University Campus.

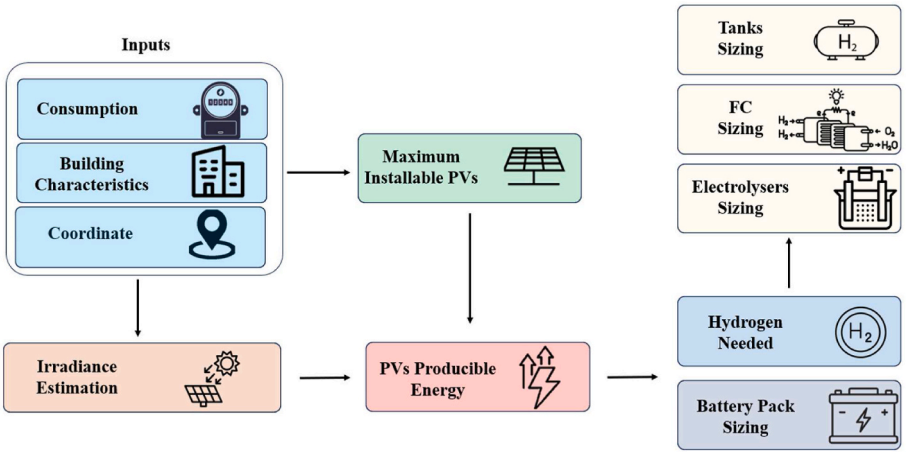

Fig. 2. Plant sizing approach.

Table 1
Available surface for PV installations.

Flat Roofs [m^2]	Solped Roofs [m^2]
3405	2364

was calculated. To account for spacing between modules, the overall available area was reduced by 10% [35]. The number of installed PVs, N (equal to 2930), was obtained by dividing the total area of the roofs, A_{PV}, by the area of the single PV module. Therefore, the theoretical annual energy production, E_{theo}, can be defined by Equation (2.1).

$$E_{theo} = \sum_{i=1}^{N} N \cdot A_{PV} \cdot \text{Irradiance} \cdot \eta_{PV} \cdot (1 - \beta) \quad (2.1)$$

Where β represents the thermal losses power losses in the cables (Joule effect) [36] and η_{PV} the efficiency of the panel defined as the ratio between the output power of the panel and the solar input power. Table 2 summarizes the characteristics of the PV module considered in this work [37]. The choice of this specific module [37] was aimed at maximizing the power-to-area ratio and efficiency compared to other available components on the market.

Then, the irradiance was calculated through the open-source software PVGIS using the location of each building, and the orientation and inclination of the PVs modules [38]. Fig. 4 represent the output of PVGIS for the two conditions, sloped and flat roots respectively.

It is important to note that the average irradiance per month accounts for the effects of both seasonality and weather. Using these data, the expected energy production was calculated for each month, with the results summarized in Table 3.

As it can be observed, the highest production is expected in July, when the irradiance reaches its peak in both flat and sloped PVs. After estimating the available energy from PVs, the consumption data was analysed. The dataset related to the energy need of the buildings spans the period between 2018 and 2021. Nevertheless, due to the significant alteration in consumption caused by the COVID pandemic (limitation in the attendance of the buildings), the data from 2020 were excluded from the analysis, avoiding a wrong plant sizing [39]. Consumption data were averaged over the years (excluding 2020) considering the structure's operation for 5 days a week and accounting for holydays such as Christmas, Easter, and the University summer break (in August). Table 4 summarizes the monthly energy consumption (electrical only) in MWh. Since the buildings have a trigeneration power plant (producing electrical power, cooling, and heating in a single plant), their energy needs are limited to electricity from the grid. As a result, the energy consumption reported in Table 4 describes the total energy needs of the buildings for this case study.

August shows the minimum consumption, while January, April and December have lower values compared to the other months, as expected. The available energy production from the PVs was reported alongside the energy consumption of the buildings in Fig. 5.

As clearly visible, the energy production is lower than consumption in January, February, October, November, and December. Additionally, there is a significant gap between the production and consumption during the end of the spring and in summer. This indicates that the energy produced from April to September must be stored for use in the other months. Furthermore, an experimental analysis on the buildings temperatures revealed inefficient air conditioning management, resulting in excessively cold temperatures in summer and overly warm temperatures in winter with respect to national guidelines for public buildings thermal management [40]. Therefore, a reduction in the consumption can reasonably be expected with smarter management. Since the power demand is directly related to the distance between external and internal temperature of the buildings, it is estimated that such improvements could reduce the total consumption by up to 20%.

Table 2
PV characteristics.

Nominal Power [W]	400
η_{PV} **[%]**	22.6
Open circuit current [A]	6.58
Open circuit voltage [V]	75.6
Power temperature coefficient [%/°C]	−0.29
Voltage temperature coefficient [mV/°C]	−176.8
Current temperature coefficient [mA/°C]	2.9
Area [m^2]	1.77

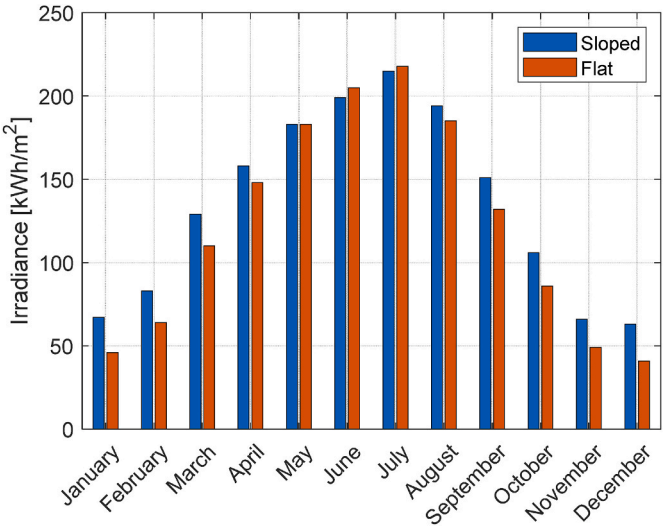

Fig. 4. Irradiance on the PVs: flat and sloped modules.

2.1.2. BP sizing

The next step involves sizing the BP. The BP capacity was determined based on the month with the largest gap between consumption and production, which is November. November has one of the lowest production rates and intensive energy consumption inside the buildings, due to low external temperatures. The capacity of the BP was calculated considering the battery's efficiency, defined as the ratio between the energy discharged and the energy charged [41]. The efficiency is influenced by various factors, including the State of Charge (SOC), the SOH, internal temperature, and discharge current [42–44]. However, for this preliminary design, a fixed efficiency (η_{BP}) of 90% [45] was assumed. Using the energy demand in November, E_{nov}, the battery capacity was calculated as shown in Equation (2.2), where the energy necessary for one month was divided by the BP efficiency and the days per month.

$$Capacity_{BatteryPack} = \frac{E_{nov}}{30 \cdot \eta_{BP}} \quad (2.2)$$

These considerations lead to a nominal capacity of the BP of about 4 MWh. However, to reduce the total cost of the plant, the capacity was halved. In this way, the BP (worst case: November with maximum energy consumption and near-zero PV energy production) is capable to sustain the energy demand for a maximum of half a day. This aspect implies other considerations on the energy management that will be discussed in the next paragraphs.

2.1.3. Hydrogen production

From the months where the energy provided by the PVs is not enough to withstand the request of the building, it is possible to estimate the amount energy needed from the FC system. Knowing the energy request (i.e., the difference between the request from the building and the provided by the PVs), the equivalent hydrogen mass can be calculated considering the Lower Heating Value (LHV) of hydrogen to be

Table 3
Expected energy production in MWh.

Jan	Feb	Mar	Apr	May	Jun	Jul	Aug	Sep	Oct	Nov	Dec
55	73	119	154	185	205	219	191	141	95	57	51

Table 4
Consumption per month in MWh.

Jan	Feb	Mar	Apr	May	Jun	Jul	Aug	Sep	Oct	Nov	Dec
86	116	119	79	116	111	112	44	109	112	113	79

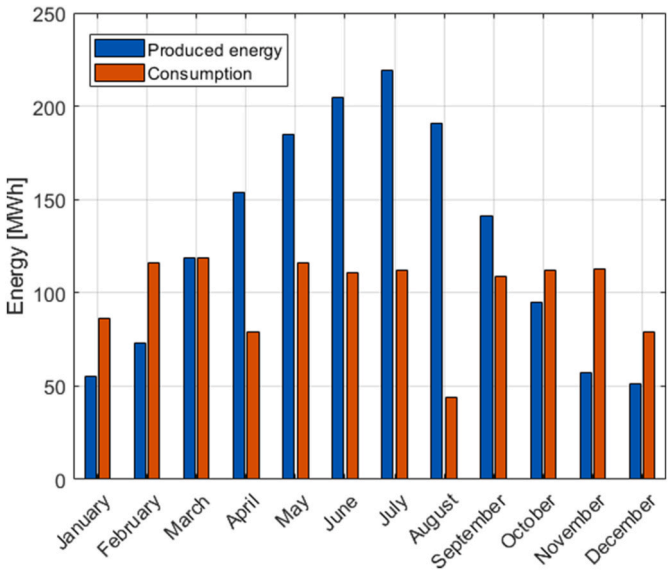

Fig. 5. Expected energy production and consumption in MWh.

33.33 kWh/kg, and assuming a combined conversion efficiency of FC and inverter (η_{FC}, $\eta_{Inverter}$) of 40.5% [46] (45% FC efficiency and 90% inverter), the amount of hydrogen needed can be estimated from Equation (2.3).

$$H_{2\ needed} = \frac{Energy_{request}}{LHV^{*}\ \eta_{FC}{}^{*}\ \eta_{Inverter}} \tag{2.3}$$

The theoretical hydrogen consumption per month is shown in Table 5. As indicated, there is no hydrogen request connected to energy consumption from the buildings between April to September. This outcome is a direct consequence of the monthly approach used. However, in a more realistic scenario, hydrogen would still be needed in small amounts during these months, when the PVs are not producing energy, and the BP is depleted (this aspect will be considered in the next paragraphs). Extended periods of cloudy days can lead to this scenario, which is not evident in the monthly-based modelling because this effect is inherently included in the overall irradiance calculations.

After calculating the hydrogen consumption, the focus can be shifted to the electrolyser. The available energy for hydrogen production was estimated by adding the extra energy from PV month-by-month to the energy generated when the structure is closed (assuming zero energy consumption during these periods). The resulting available energy per month is shown in Table 6. This approach indicates that hydrogen production would also occur in winter, since the structure is only open five days a week.

The sizing of the electrolysers was conducted based on the month with the maximum available energy for the electrolysis, which is August. During this time, the buildings are closed for an extended period of time and solar power production is near its peak. For this case study, the energy consumption of the electrolysers (energy required from the electrolyser per kg of hydrogen produced) was set to 55 kWh/kg, as the average energy consumption of commercial electrolysers available in the market [47,48]. Consequently, the expected hydrogen production in August is estimated to be 4050 kg. Next, the hydrogen mass flow rate was calculated over 30 days, resulting in 5.66 kg/h. Based on these data, an appropriate electrolyser (main electrolyser) was identified on the market, whose characteristics are summarized in Table 7 [49].

The nominal flow rate can be converted to a mass flow rate using the density, resulting in 1.79 kg/h. To obtain the aforementioned hydrogen mass, four electrolysers are required. However, since the efficiency of an electrolyser depends on the operating conditions [50], it was decided to select electrolysers of different sizes to maximize the hydrogen production efficiency of the system, even when the available energy is limited (minimizing the off-design operative conditions). Specifically, a smaller electrolyser was added to operate alongside the others. This smaller device will be used during high peaks of PV production or in the winter months. The technical characteristics of the secondary electrolyser are summarized in Table 8 [49].

Once the devices for hydrogen production were defined, the mass flow rates for the summer and winter months were calculated to be 8.1 kg/h and 2.7 kg/h, respectively, with corresponding power consumption of 450 kW and 150 kW. Finally, the expected hydrogen production was determined based on the available energy from PV, energy requests of the buildings (which defines the maximum operating hours), and the hydrogen mass flow rate. Table 9 summarizes the hydrogen production in kg.

The comparison between the monthly-based requested (Table 5) and produced (Table 9) hydrogen, reported in Fig. 6, clearly shows different trends under the hypothesis of this theoretical analysis.

For instance, in January the request exceeds the production. However, the overall production is higher than the request. Therefore, it is evident that a storage system is essential to maximize the benefits of the hydrogen-based energy plant previously mentioned.

2.1.4. Hydrogen storage & compressor sizing

Among different solutions for hydrogen storage, due to the high reliability and the low complexity, compressed gaseous storage was selected in this case study. The storage systems consist of three main components: a high-pressure storage tank, a volumetric compressor, and a buffer tank (needed to dampen the mass flow oscillations from the

Table 5
Theoretical Hydrogen consumption in kg.

Jan	Feb	Mar	Apr	May	Jun	Jul	Aug	Sep	Oct	Nov	Dec
2270	3186	743	0	0	0	0	0	0	1778	3878	2066

Table 6
Available energy for electrolysis in MWh.

Jan	Feb	Mar	Apr	May	Jun	Jul	Aug	Sep	Oct	Nov	Dec
22	17	29	116	91	119	133	226	48	23	14	20

Table 7
Main electrolyser technical characteristics.

Nominal Flow Rate [Nm^3/h]	20
Outlet pressure [bar]	30
Power request @ maximum flow rate [kW]	100

Table 8
Secondary electrolyser technical characteristics.

Nominal Flow Rate [Nm^3/h]	10
Outlet pressure [bar]	30
Power request @ maximum flow rate [kW]	50

electrolyser and prevent damage to the compressor). The total volume of the buffer tank was set to 40 m^3. The compressor was then selected, based on the range of intake pressure, outlet pressure, and the flow rate (which must be compliant with the outputs of the electrolysers). For this case study, a dual-stage volumetric compressor was selected from the market. The main characteristics of the compressor are summarized in Table 10 [51].

The energy required by the compressor can be evaluated by estimating the number of operating hours (based on available energy from PV, hydrogen to be compressed, and nominal power consumption of the compressor). The results are presented in Table 11.

This energy must be subtracted from the amount of energy available for hydrogen production, as the objective of this work is to design an off-grid power system. Consequently, there is a slight reduction in the total hydrogen produced because the energy available from the PV was lower. Table 12 presents the updated values.

Regarding the volume of the high-pressure storage system, the maximum overall hydrogen quantity was considered (taking into account hydrogen consumed and produced), starting from April. This value was then used to size the volume of the tanks at 350 bar (nominal operating pressure). Fig. 7 shows the evolution of the hydrogen storage level starting from April.

September is the month when the storage reaches its maximum capacity, as hydrogen consumption in preceding months is limited. This results in a tank overall volume of approximately 460 m^3 (13000 kg of compressed hydrogen at 350 bar).

2.1.5. FC sizing

Finally, the FC was sized on the assumption of recharging the BP. A PEM FC was chosen due to its ability to achieve higher efficiencies [52–55] and its compatibility with the hydrogen grade produced by PEM electrolysers. Despite Solid Oxide Fuel Cells (SOFCs) present higher efficiencies [56] with respect to PEM FC, their potential can be exploited in cogeneration applications. Since in the present work it has been decided not to modify the installed power plant (trigeneration plant feed with electrical energy), SOFCs have not been considered. As regards the FC sizing, in a worst-case scenario, where the battery is completely discharged after 1 day, the BP should be recharged up to 50% SOC between 9:00 p.m. and 8:00 a.m. of the next day from the FC. Since the BP was sized with a nominal capacity of 2 MWh, the FC must be able to deliver at least 1 MWh to the BP during this period of time. Moreover, considering the month with the highest energy consumption in the buildings, up to 2 recharging cycles per day were assumed, totalling four recharges. After the night recharge (resulting in 50% SOC), if the PVs can meet the building energy demands, the FC remains idle. However, given the BP's capacity, it can last 3 h and 15 min without FC or PV energy. For this reason, FC power was seized accordingly to deliver 1 MWh in 3 h and 15 min, resulting in a nominal power of 310 kW (capable of following the power requests of the buildings for a reasonable amount of time). It is important to underline that the direct use of solar power (if extra power from PV is available) should be prioritized for BP charging (with respect to FC), due to its higher efficiency. For this case study, commercial FCs with nominal powers of 200 kW and 150 kW were selected to always try to maximize efficiency based on power request [57]. Additionally, a DC/DC converter and its efficiency must be considered for direct BP recharging using hydrogen during the nights.

2.2. Plant modelling

In this subsection, the modelling of the plant will be presented. A 0-D dynamic model was developed in MATLAB/Simulink to observe the plant's performance over an entire year, with a resolution of 5 min. To make the simulation as realistic as possible, the model incorporates

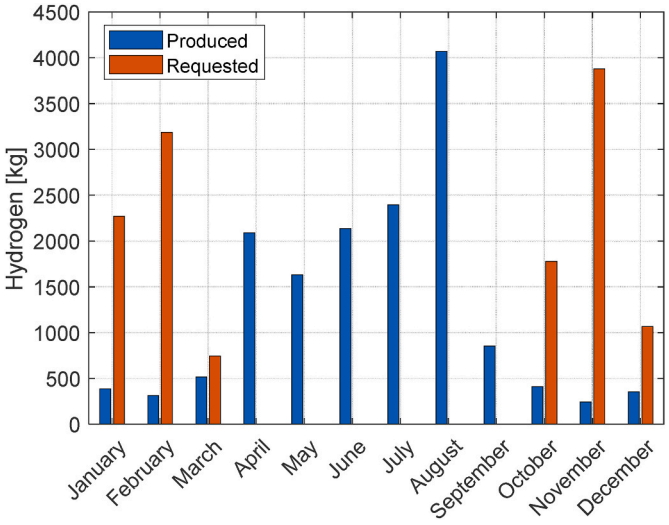

Fig. 6. Comparison between produced and requested hydrogen.

Table 10
Compressor characteristics.

Intake Pressure [barA]	Up to 31 bar
Maximum discharge pressure [barA]	351
Nominal flow rate [Nm^3/h]	20
Absorbed power [kW]	11

Table 9
Expected hydrogen production in kg.

Jan	Feb	Mar	Apr	May	Jun	Jul	Aug	Sep	Oct	Nov	Dec
388	314	514	2087	1631	2136	2396	4068	855	411	245	356

Table 11
Compressor energy demand in kWh.

Jan	Feb	Mar	Apr	May	Jun	Jul	Aug	Sep	Oct	Nov	Dec
88	71	116	472	369	483	541	919	193	93	55	80

Table 12
Net Hydrogen production in kg.

Jan	Feb	Mar	Apr	May	Jun	Jul	Aug	Sep	Oct	Nov	Dec
386	313	512	2079	1625	2128	2387	4052	851	410	244	355

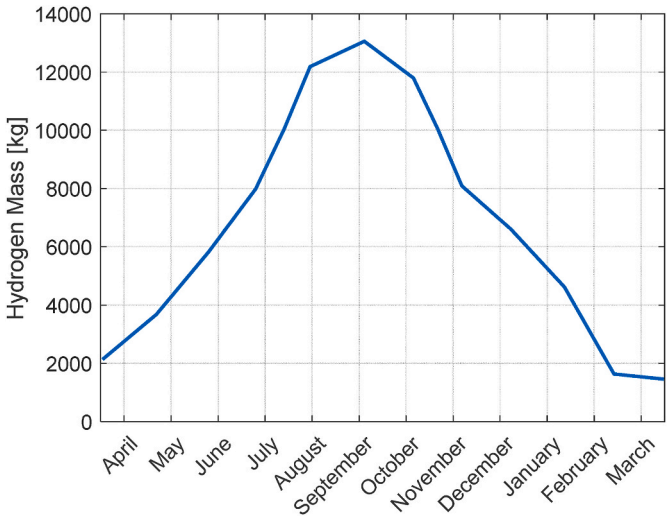

Fig. 7. Hydrogen storage level from April.

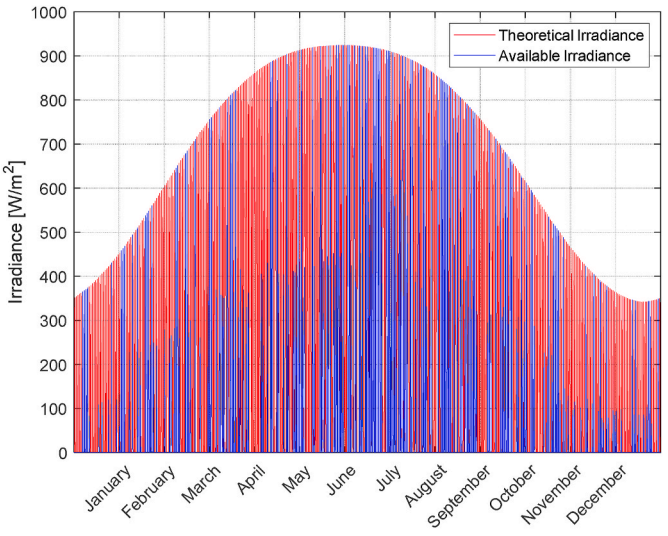

Fig. 8. Theoretical (red) and statistical (blue) irradiance. (For interpretation of the references to colour in this figure legend, the reader is referred to the Web version of this article.)

time-based irradiance profiles as inputs.

2.2.1. *Weather generator*

Weather conditions significantly impact the irradiance available to the PVs. As it is well-known, irradiance is not only a determined by geographical location and seasonality, but it is also affected by weather events (e.g., clouds, rain, fog …). The theoretical irradiance (represented by the red trace in Fig. 8), estimated through a model [58], serves as input for a specifically developed weather generator. This generator adjusts the available irradiance based on the average number of cloudy and partly cloudy days per month, using a set of coefficients. These coefficients range between 1(clear sky) and 0 (completely cloudy), reflecting the degree of sky coverage.

As observed in Fig. 8, the statistical irradiance estimated using the weather generator consistently remains lower than the theoretical irradiance. This difference is especially pronounced during the winter months, due to the increase of cloudy or rainy weather days.

2.2.2. *Consumption profiles*

The second stage of modelling focused on generating time-based energy consumption profiles. In the previous section, energy demand was presented as monthly averages, which were used for preliminary considerations (components sizing and layout), but lacked details required for more realistic scenarios. To address this issue, an energy consumption coefficient was introduced to account for varying energy needs throughout the day in the buildings. The daily energy consumption, calculated as the monthly total divided by the number of opening days, Fig. 9, was divided into three time-resolved levels.

- Low (8:00 p.m. to 7:00 a.m.): during these hours, when the structure is closed to the public, energy demand is considered minimal or zero, depending on whether a theoretical or more realistic scenario is being considered.
- Mid (7:00 p.m. to 8:00 p.m. and 6:00 a.m. to 7:00 a.m.): these periods reflect transitional stages where the structure is either closing or about to open. At 7:00 p.m. to 8:00 p.m., cooling/heating systems are typically off, while lighting may still be in use. From 6:00 a.m. to

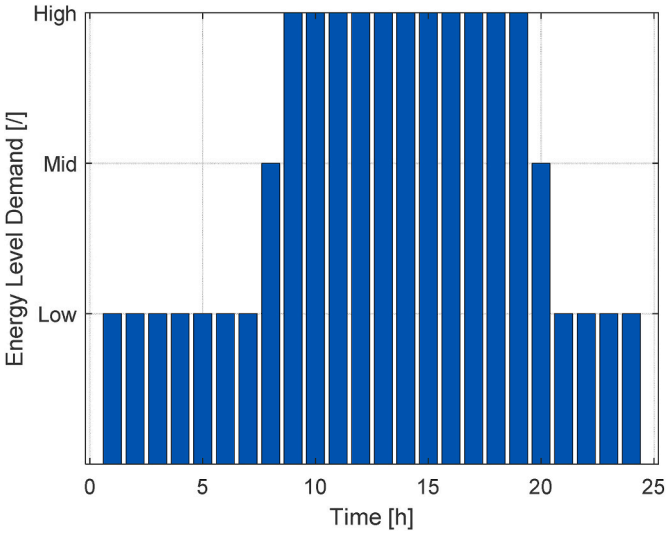

Fig. 9. Daily energy consumption levels.

7:00 a.m., heating/cooling systems begin warming-up the building before full operation, without activating lighting systems.
- High (7:00 a.m. to 8:00 p.m.): this is the period of full operational load for the structure.

2.2.3. Solar energy production modelling

The first component considered in the 0-D model is the PV system. Initially, the theoretical maximum current and voltage were adjusted, based on the difference between the statistical irradiance and the theoretical irradiance. Subsequently, these adjusted values were further scaled by a coefficient that considers the temperature of the PV cells. These steps yield the power output of each PV panel. With the power output known for a single panel and the configuration of the PV array, the total energy production can be estimated (Equation (1.1)).

2.2.4. BP modelling

As described above, the power entering the BP (P_{batt}) was calculated using Equation (2.4), where $P_{produced}$ represents the power produced from the PVs, P_{FC} the power produced by the FC, P_{user} is the power delivered to the user and $P_{compressor}$ the power drained by the compressor.

$$P_{batt} = P_{produced} + P_{FC} - P_{user} - P_{compressor} \tag{2.4}$$

The BP consists of four individual packs 500 kWh each. When the first pack reaches its maximum capacity, the system starts charging the subsequent packs sequentially, until the last one is fully charged. During discharge, the first pack to be discharged is the last that was previously charged. This charging/discharging sequence is detrimental to the SOH of the BP [59]. Therefore, the packs are inverted every thirteen weeks to avoid unbalanced degradation of each pack.

2.2.5. Electrolyser modelling

The electrolyser was modelled as follows: the net power available for the electrolysis is calculated by Equation (2.5). When the BP is fully charged, this power is further multiplied by the efficiency of the inverter, as in Equation (2.5).

$$P_{electrolysis} = \left(P_{produced} - P_{user} - P_{compressor}\right) * \eta_{inverter} \tag{2.5}$$

Once the instantaneous power available for the electrolysis was calculated, the instantaneous hydrogen demand was determined using Equation (2.6), where $P2H_2$ represents the amount of power needed to obtain one normal cubic meter of hydrogen per hour.

$$H_{2\ flow} = \frac{P_{electrolysis}}{P2H_2} \tag{2.6}$$

2.2.6. Buffer tank and hydrogen compressor modelling

The buffer tank was modelled as a vessel with a volume of 40 m^3, which follows the ideal gas law, ensuring the pressure does not exceed 30 bar. During the plant design, it was decided that the minimum volume of hydrogen stored in the buffer tank should not drop below 100 Nm^3. This threshold ensures having sufficient hydrogen to dampen the oscillations in the tank. To manage the compressor, a simplified management strategy was adopted: the compressor is switched on when the level of the buffer tank exceeds a user-defined threshold. Since the compressor is considered one of the most hazardous components of the hydrogen system, the use of a simplified strategy allowed increasing the reliability of the hydrogen production and storage system even in case of issues.

2.2.7. Hydrogen high pressure storage modelling

As already discussed, the maximum storage pressure was set to 350 bar. The mass variation within the tank can be calculated multiplying the mass flow rate by the simulation step size. It is important to underline that this flow rate can be positive (when hydrogen is pumped into the tank by the compressor) or negative (when hydrogen is drained from the tank during FC operation). Thus, the mass of hydrogen stored in the tank is known at every moment and the storage pressure (and its filling level) can be estimated from the ideal gas law. This information is crucial for a proper management of the system. The main storage system was modelled using two equations: Equation (2.7) defines the instantaneous mass of hydrogen transferred to the main storage, calculated as the product between the instantaneous volumetric flow rate from the compressor, the step time and the density of hydrogen, while Equation (2.8) delivers the actual pressure and the volume of the tank. In this case study, the volume of the tank was set to 500 m^3 (from the sizing was resulting 460 m^3).

$$m_{H2} = Q_{compressor} * \Delta t * \rho_{H2} \tag{2.7}$$

$$p_{tank} = \frac{m_{H2\ stored} * R * T_{tank}}{MM_{H2} * V_{tank}} \tag{2.8}$$

Under these assumptions and using physical relations between different systems, the model was able to accurately predict the amount of hydrogen stored in the tank and the pressure variations due to emptying/filling process.

2.2.8. Fuel Cell modelling

The modelling of the FC was kept as simple as possible, to focus on providing information about the overall performance of the plant, rather than on a detailed description of the component's behaviour.

Therefore, the FC model subsystem was focused on the determination of the hydrogen demand to produce a target energy output. As a matter of fact, given the FC efficiency, the hydrogen needed was calculated using Equation (1.9).

$$m_{H2\ needed} = \frac{Energy_{request}}{LHV * \eta_{FC} * \eta_{Inverter}} \tag{2.9}$$

Table 13 summarizes the sizing of each component in the final configuration of the energy plant.

2.3. Control strategy

The previous sections presented the modelling of each component. However, to maximize the efficiency of the system, the development of a dedicated control strategy represents a key point of this case study. Energy flows have to be managed to deliver the requested energy to the buildings and components without compromising the overall efficiency. Moreover, specific controls allow to guarantee a safe, correct, and reliable operation of the plant.

The first monitoring process concerns the net power available from the PV. To maximize the conversion efficiency, this energy has to be directly supplied to the buildings or spent on the compressor and electrolysers (if extra energy is available). Then, several scenarios come into play. First, the control assesses if the extra energy can be stored in the BP without exceeding its nominal capacity. In fact, this option is always preferable as it will maximize the overall storage efficiency. Therefore, two options are available (considering the available energy produced from the PVs decurted of the BP recharging efficiency).

- SOC + available energy < BP nominal capacity: the BP will be charged.
- SOC + available energy > BP nominal capacity: the BP would be charged up to 100% SOC and the remaining energy will be sent to the electrolysers.

The strategy also evaluates the SOH of the BP which should be always preserved. As a matter of fact, many cycles and high levels of Depth of Discharge (DOD), defined as in Equation (2.10), can affect the overall expected life of the BP.

$$DOD = 100 - SOC \tag{2.10}$$

Table 13
Summary of the main component sizes in the final energy plant layout.

Component	Number [/]	Power consumption [kW]	Energy Capacity [MWh]	Nominal Flow Rate [N m^3/h]	Storage Capacity [m^3]
PV	2930	/	/	/	/
BP	1	/	2	/	/
Main electrolyser	1	100	/	20	/
Secondary electrolyser	1	50	/	10	/
Compressor	1	11	/	20	
Buffer tank	1	/	/	/	40
Main storage (350 bar)	1	/	/	/	500

Two controls were then implemented: firstly, since the BP is made of several modules (4 in this case study), the charging/discharging order of the modules will be changed cyclically 4 times per year (every 13 weeks), allowing to balance the SOH of the batteries within the BP. Further optimization could be achieved concerning the swapping order: for instance, monthly changes in the DOD of the battery pack may be taken into account. Moreover, to avoid impacts on the SOH, the DOD was limited to a maximum of 95%, corresponding to a minimum SOC of 5%. In addition to this, the electrolysers have also to be properly managed.

As previously discussed, for an efficient hydrogen production rate two different sizes are employed: larger units (main electrolysers) will be activated during summer to maximize hydrogen production from excess PV energy, while smaller units (secondary electrolysers) are used during other months, to optimize the hydrogen production efficiency. The management of the compressor and buffer tank filling was synergically coordinated: the level of the buffer tank triggers the compressor operation. Indeed, the compressor operates when the buffer tank reaches 50% capacity and stops when it drops to 20%, to prevent damage.

Finally, the FC operation was optimized as follows: it recharges the BP during nights reaching SOC 50%, when the energy demand combined with the production deplete the BP below this threshold or feeds directly the building when peak power (higher than battery peak power) are requested.

3. Results and discussion

This section presents the results in terms of energy flows and hydrogen production/consumption using the 0-D dynamic model of the hydrogen-based energy plant in working conditions for this case study. This approach allows for the simulation of various configurations, highlighting potential issues in component sizing or the overall viability of the plant, thereby saving costs and time. Of particular interest is the comparison of the energy and hydrogen production with respect to the data calculated from the monthly-based sizing approach.

Initially, the model was simplified introducing three hypotheses (which will be removed in the next section).

- Consumption during closing periods was assumed to be negligible
- The influence of the temperature on the PVs production was neglected
- The minimum allowed SOC of the BP was set to 0%.

These hypotheses were made to compare the results of the model with respect to monthly-based evaluations. As a result, the 0-D dynamic model was fed both with monthly and instantaneous data.

Fig. 10 shows the comparison between the two irradiance profiles sent to the model. The red trace shows a constant trend per month, while the blue lines alternate high peaks to zero values. Despite the different distributions, the total energy remains consistent across both modelling strategies (as visible in Fig. 11).

The initial comparison focused on the available energy from the PV, as shown in Fig. 11. The graph depicts the energy production from PV using the daily averaged data from the sizing procedure (blue line), the

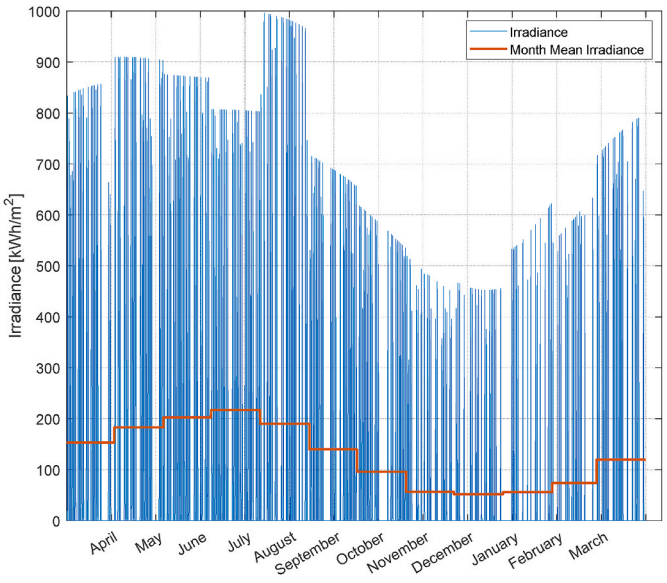

Fig. 10. Comparison between instantaneous and monthly-average irradiance profiles.

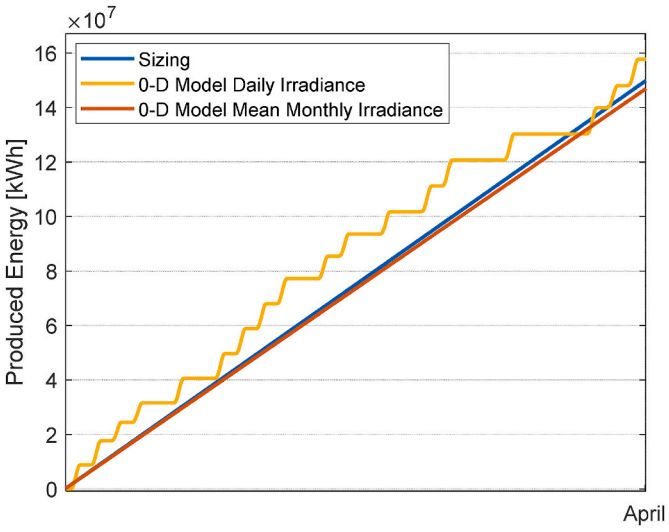

Fig. 11. Energy Production form PV in April.

monthly averaged data (red line) and the instantaneous data (yellow line) for the month of April. It is evident that the three methods exhibit similar trends and converge toward the same value. As expected, the blue and the red lines closely align due to their constant profiles (consistent slopes). In contrast, the yellow line shows higher production rates and periods of constant energy (related to the bad weather days).

Moreover, it is interesting to evaluate the energy production from PV

over 1 year, as shown in Fig. 12.

The profiles are similar and, also in this case, tend to the same value. Nonetheless, small differences are discernible, largely attributable to the weather generator. In fact, the yellow profile displays a step-like pattern, due to nights and varying weather conditions that result in periods of no PV production. Following the validation of energy production, the net energy available for the electrolysers, shown in Fig. 13, was analysed. While all the traces converge to the same value, variations in slopes between them can be observed.

Finally, the hydrogen production was analysed and reported in Fig. 14. According to previous trends, the final values for the three modelling methodologies show remarkable similarity.

Despite energy production from PV, net energy, and hydrogen production show similar behaviour among the tree modelling strategies, the analysis of the requested mass of hydrogen depicted in Fig. 15 shows remarkable differences. Notably, due to the sizing approach employed, using the monthly averaged data the hydrogen request remains equal to zero for six months. On the other hand, differences between the monthly averaged data (red line) and the instantaneous data (yellow line) result in a significantly different shape for hydrogen demand in power generation.

The three approaches lead to the same total amount of hydrogen needed. However, the blue curve indicates zero demand for several months: this is related to the mean modelling of the power system performed in this study.

As a final step, the three initial hypotheses (ideal PV system, minimum SOC of 0% and average energy consumption of the buildings) were removed to study how the hybrid solar-hydrogen power system and controllers would behave in more realistic conditions. This led to the following considerations.

- Energy production was decreased by approximately 7% due to the temperature effect on the PVs;
- Energy consumption of the building increased by about 20% because the energy consumption level during nights was set to low level (instead of zero);
- The minimum achievable SOC is set to 5%, to optimize the SOH of the BP.

Under these more realistic conditions, the 0-D model of the hybrid solar-hydrogen power system shows a 6 % reduction in the total energy produced, as shown in Fig. 16.

This decrease in total energy production is due to the reduced efficiency of the PV system caused by the temperature effect. Consequently, this significantly impacts the energy available for electrolysis and, therefore, the amount of hydrogen produced, as reported in Fig. 17.

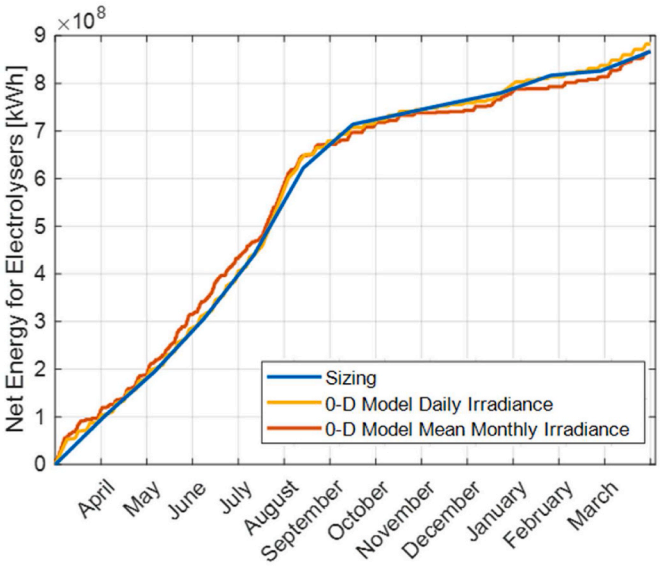

Fig. 13. Net Energy available for the electrolysers.

In addition to this, the hydrogen request increases because the more realistic conditions reduce the overall efficiency, thereby increasing the amount of energy needed from electrolysers and compressor. Finally, the difference between the required and the produced hydrogen was calculated (starting from April) and shown in Fig. 17. Under the hypothesis previously discussed, the gap results in 2700 kg (14600 kg requested against 11900 kg produced), which means that the more realistic scenario requires a higher amount of PV or higher capacity of the BP. However, since this case study describes a preliminary design of hybrid solar-hydrogen power system, a difference of 14 % between requested and produced hydrogen can be considered acceptable.

Fig. 18 shows the comparison between requested and produced hydrogen with the same plant previously presented but with an increased (+50%) capacity of the BP. As expected, the higher the storage capacity, the lower the hydrogen demand, thus the matching between requested and supplied hydrogen can be achieved at the end of the year.

Another possible option is the increase of the number PV modules. This would result in an increase of 350 modules in the PV array. The output of the model reported in Fig. 19 indicates that hydrogen production can exceed the requested values throughout the year.

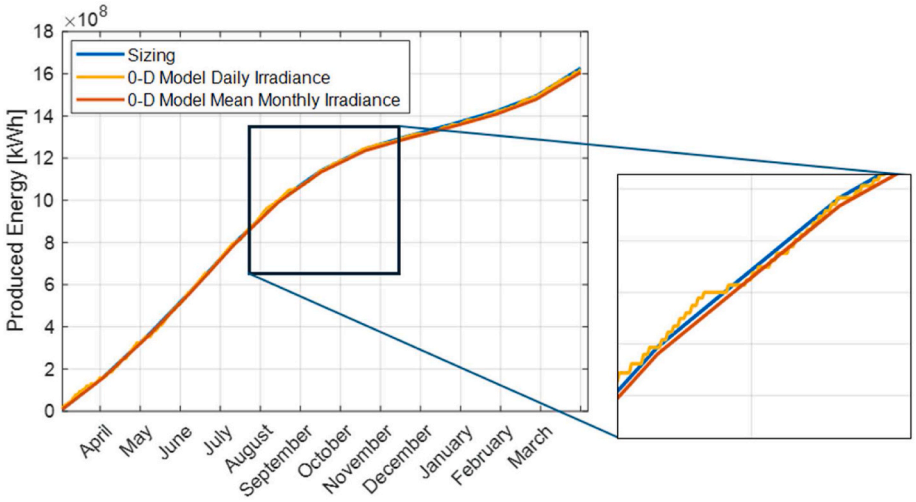

Fig. 12. Energy production from PV over 1 year.

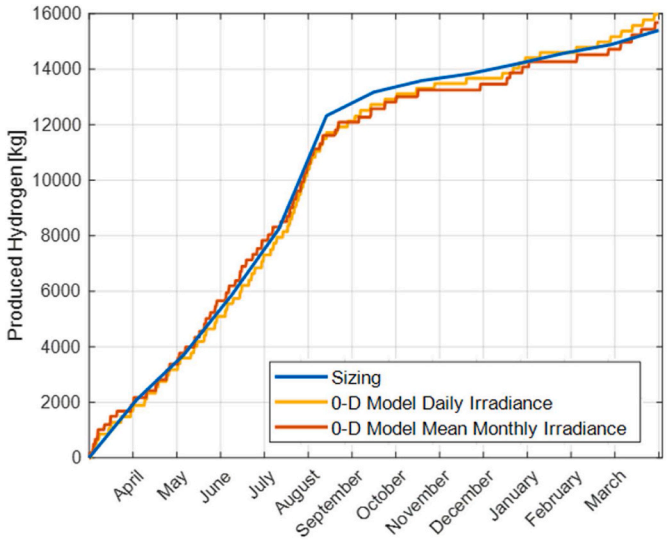

Fig. 14. Hydrogen production.

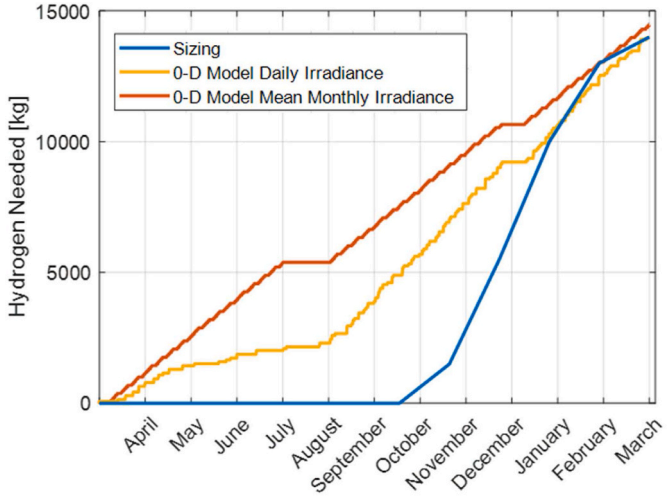

Fig. 15. Hydrogen needed.

As it can be clearly seen, both methods ensure the complete independence of the structures. However, the second approach results in overproduction, leading to a surplus of hydrogen stored at the beginning of the next year (starting from April).

4. Conclusions & future developments

This paper presents a design framework for off-grid hybrid solar-hydrogen energy plant. The case study of this work is focused on an academic teaching building complex at the University of Bologna, Italy. Initially, the plant was designed using average values of energy needs over the year per months, with emphasis on component sizing, irradiance estimation and energy consumption evaluations. The proposed design pathway allowed to identify the most convenient configuration of the plant in terms of sizing and device interactions for achieving complete grid independence. Subsequently, the same components were described and coupled in 0-D dynamic model using a simulation environment, allowing to run time-based simulations with 5-min resolution. Dedicated control strategies were implemented to enhance efficiency and optimize energy flows using different inputs of irradiance and energy demand (constant and variable daily consumption levels) in the buildings. The main outcome of the analysis demonstrates a good

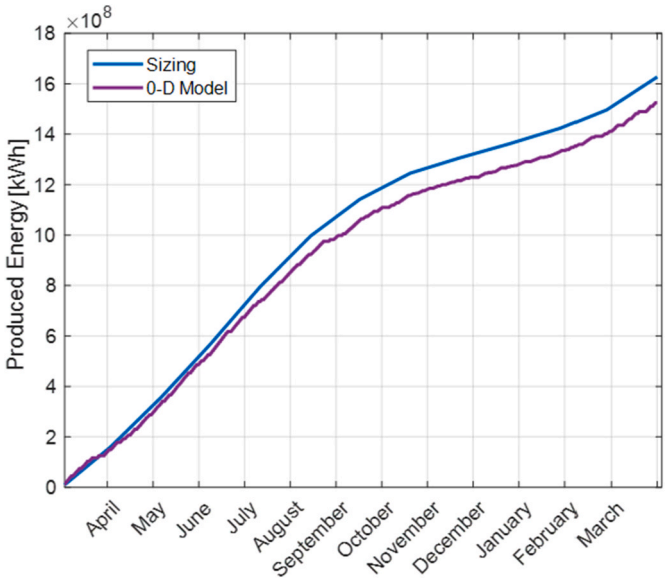

Fig. 16. Energy production considering real conditions.

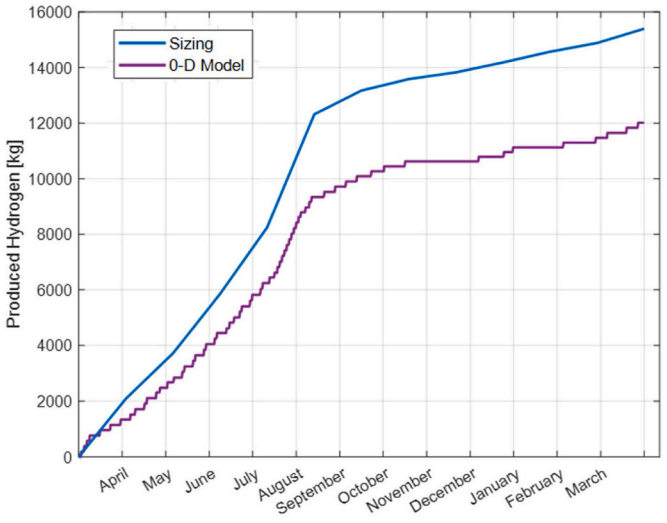

Fig. 17. Hydrogen production considering real conditions.

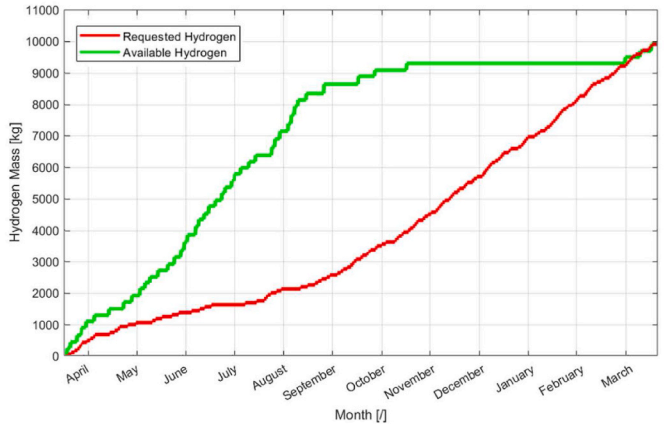

Fig. 18. Hydrogen production and requested with an increase of 50% of the BP capacity.

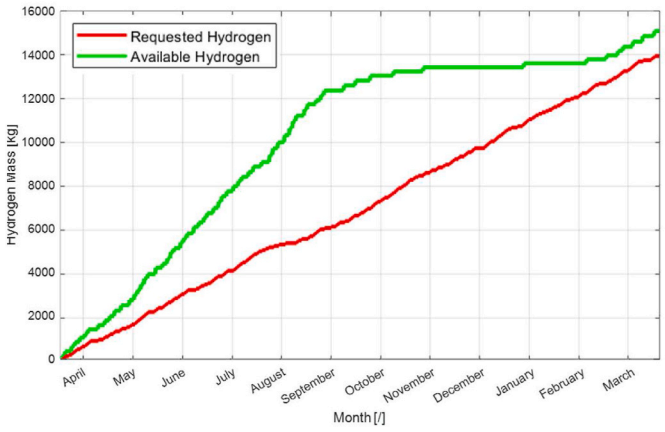

Fig. 19. Hydrogen production and requested with an increase of the installed modules.

accordance between the different sizing approaches (monthly average, mean-daily, and daily) along the year.

Remarkable distance in both energy availability from PV (+7%) and hydrogen production and consumption rates were observed moving from the first sizing in a simplified scenario (mean monthly values) to the more realistic scenario considered in this work (daily values). The results demonstrated good accuracy in estimating energy production from PV, the energy needed for electrolysis, and the hydrogen compression and storage process. Moreover, by analysing the model outputs under a realistic scenario, the need for modifications in the plant layout to meet varying energy demands emerged. Two possible approaches aimed at ensuring the complete independence from the grid for the buildings (modifications on the PV sizing and BP) were proposed and the outputs of the 0-D energy plant model confirmed the importance of proper sizing of each component to avoid extra hydrogen production. The design methodology, coupled with the energy flow predictions obtained through the 3-D model of the plant proposed in this paper, aims to describe different power plant layouts and sizes while assessing the feasibility, performance, and costs of various technical solutions.

Future developments might be addressed at enhancing the modelling of the individual components, such as FCs and electrolysers. Additionally, more complex layout could be investigated, including the introduction of wind power generation, secondary energy flows for thermal needs (heat and cold), and auxiliaries. Finally, the estimation of water consumption for the electrolysis process, carbon footprint evaluations, recovery from exhaust gases of the FC could be explored to provide a comprehensive LCA analysis of a generic hybrid hydrogen-solar energy plant.

CRediT authorship contribution statement

Pier Paolo Brancaleoni: Writing – original draft, Visualization, Methodology, Investigation, Data curation, Conceptualization. **Giacomo Silvagni:** Writing – review & editing, Supervision, Methodology, Investigation, Formal analysis, Conceptualization. **Vittorio Ravaglioli:** Writing – review & editing, Supervision, Resources, Funding acquisition. **Enrico Corti:** Writing – review & editing, Supervision, Resources, Methodology. **Davide Moro:** Writing – review & editing, Resources, Project administration, Funding acquisition.

Declaration of competing interest

The authors declare that they have no known competing financial interests or personal relationships that could have appeared to influence the work reported in this paper.

References

[1] Holdren JP. Population and the energy problem. Popul Environ Mar. 1991;12(3):231–55. https://doi.org/10.1007/BF01357916.
[2] Renewable energy targets - European Commission. Accessed: Jan. 29, https://energy.ec.europa.eu/topics/renewable-energy/renewable-energy-directive-targets-and-rules/renewable-energy-targets_en; 2024.
[3] 'Renewables - Energy System', IEA. Accessed: January. 29, 2024. [Online]. Available:.https://www.iea.org/energy-system/renewables.
[4] Pubblicazioni statistiche - terna spa. https://www.terna.it/it/sistema-elettrico/statistiche/pubblicazioni-statistiche. [Accessed 24 January 2024].
[5] Clò S, Cataldi A, Zoppoli P. The merit-order effect in the Italian power market: the impact of solar and wind generation on national wholesale electricity prices. Energy Pol Feb. 2015;77:79–88. https://doi.org/10.1016/j.enpol.2014.11.038.
[6] Trainer T. Some problems in storing renewable energy. Energy Pol Nov. 2017;110:386–93. https://doi.org/10.1016/j.enpol.2017.07.061.
[7] Dehghani-Sanij AR, Tharumalingam E, Dusseault MB, Fraser R. Study of energy storage systems and environmental challenges of batteries. Renew Sustain Energy Rev Apr. 2019;104:192–208. https://doi.org/10.1016/j.rser.2019.01.023.
[8] Gray E MacA, Webb CJ, Andrews J, Shabani B, Tsai PJ, Chan SLI. Hydrogen storage for off-grid power supply. Int J Hydrogen Energy Jan. 2011;36(1):654–63. https://doi.org/10.1016/j.ijhydene.2010.09.051.
[9] Marocco P, Ferrero D, Lanzini A, Santarelli M. Optimal design of stand-alone solutions based on RES + hydrogen storage feeding off-grid communities. Energy Convers Manag Jun. 2021;238:114147. https://doi.org/10.1016/j.enconman.2021.114147.
[10] Kothari R, Buddhi D, Sawhney RL. Comparison of environmental and economic aspects of various hydrogen production methods. Renew Sustain Energy Rev Feb. 2008;12(2):553–63. https://doi.org/10.1016/j.rser.2006.07.012.
[11] Nikolaidis P, Poullikkas A. A comparative overview of hydrogen production processes. Renew Sustain Energy Rev Jan. 2017;67:597–611. https://doi.org/10.1016/j.rser.2016.09.044.
[12] Wilberforce T, Olabi AG, Sayed ET, Elsaid K, Abdelkareem MA. Progress in carbon capture technologies. Sci Total Environ Mar. 2021;761:143203. https://doi.org/10.1016/j.scitotenv.2020.143203.
[13] Lane B, Reed J, Shaffer B, Samuelsen S. Forecasting renewable hydrogen production technology shares under cost uncertainty. Int J Hydrogen Energy Aug. 2021;46(54):27293–306. https://doi.org/10.1016/j.ijhydene.2021.06.012.
[14] Shiva Kumar S, Himabindu V. Hydrogen production by PEM water electrolysis – a review. Materials Science for Energy Technologies Dec. 2019;2(3):442–54. https://doi.org/10.1016/j.mset.2019.03.002.
[15] Yanxing Z, Maoqiong G, Yuan Z, Xueqiang D, Jun S. Thermodynamics analysis of hydrogen storage based on compressed gaseous hydrogen, liquid hydrogen and cryo-compressed hydrogen. Int J Hydrogen Energy Jun. 2019;44(31):16833–40. https://doi.org/10.1016/j.ijhydene.2019.04.207.
[16] Hydrogen storage methods | the science of nature. https://link.springer.com/article/10.1007/s00114-004-0516-x. [Accessed 24 January 2024].
[17] Tarhan C, Çil MA. A study on hydrogen, the clean energy of the future: hydrogen storage methods. J Energy Storage Aug. 2021;40:102676. https://doi.org/10.1016/j.est.2021.102676.
[18] Sakintuna B, Lamaridarkrim F, Hirscher M. 'Metal hydride materials for solid hydrogen storage: a review☆'. Int J Hydrogen Energy Jun. 2007;32(9):1121–40. https://doi.org/10.1016/j.ijhydene.2006.11.022.
[19] Aziz M. Liquid hydrogen: a review on liquefaction, storage, transportation, and safety. Energies Jan. 2021;14(18). https://doi.org/10.3390/en14185917. Art. no. 18.
[20] Arsie I, et al. A new generation of hydrogen-fueled hybrid propulsion systems for the urban mobility of the future. Energies Dec. 2023;17(1):34. https://doi.org/10.3390/en17010034.
[21] Zhao Y, McDonell V, Samuelsen S. Influence of hydrogen addition to pipeline natural gas on the combustion performance of a cooktop burner. Int J Hydrogen Energy May 2019;44(23):12239–53. https://doi.org/10.1016/j.ijhydene.2019.03.100.
[22] Cappelletti A, Martelli F. Investigation of a pure hydrogen fueled gas turbine burner. Int J Hydrogen Energy Apr. 2017;42(15):10513–23. https://doi.org/10.1016/j.ijhydene.2017.02.104.
[23] Lucia U. Overview on fuel cells. Renew Sustain Energy Rev Feb. 2014;30:164–9. https://doi.org/10.1016/j.rser.2013.09.025.
[24] 'Fuel cell systems: efficient, flexible energy conversion for the 21st century | IEEE Journals & Magazine | IEEE Xplore'. Accessed: January. 24, 2024. [Online]. Available: https://ieeexplore.ieee.org/abstract/document/975914.
[25] Zhang F, Thanapalan K, Procter A, Carr S, Maddy J, Premier G. Power management control for off-grid solar hydrogen production and utilisation system. Int J Hydrogen Energy Apr. 2013;38(11):4334–41. https://doi.org/10.1016/j.ijhydene.2013.01.175.
[26] Lu J, Li M, Li Q. Modeling and optimal design of a grid-independent solutions based on solar-hydrogen storage feeding green building by optimization algorithm. J Energy Storage Jun. 2023;62:106844. https://doi.org/10.1016/j.est.2023.106844.
[27] Viteri JP, Viteri S, Alvarez-Vasco C, Henao F. A systematic review on green hydrogen for off-grid communities –technologies, advantages, and limitations. Int J Hydrogen Energy Jun. 2023;48(52):19751–71. https://doi.org/10.1016/j.ijhydene.2023.02.078.
[28] Puranen P, Kosonen A, Ahola J. Technical feasibility evaluation of a solar PV based off-grid domestic energy system with battery and hydrogen energy storage in

northern climates. Sol Energy Jan. 2021;213:246–59. https://doi.org/10.1016/j.solener.2020.10.089.
[29] Guinot B, et al. Techno-economic study of a PV-hydrogen-battery hybrid system for off-grid power supply: impact of performances' ageing on optimal system sizing and competitiveness. Int J Hydrogen Energy Jan. 2015;40(1):623–32. https://doi.org/10.1016/j.ijhydene.2014.11.007.
[30] Babatunde OM, Munda JL, Hamam Y. Off-grid hybrid photovoltaic – micro wind turbine renewable energy system with hydrogen and battery storage: effects of sun tracking technologies. Energy Convers Manag Mar. 2022;255:115335. https://doi.org/10.1016/j.enconman.2022.115335.
[31] Abdin Z, Mérida W. Hybrid energy systems for off-grid power supply and hydrogen production based on renewable energy: a techno-economic analysis. Energy Convers Manag Sep. 2019;196:1068–79. https://doi.org/10.1016/j.enconman.2019.06.068.
[32] Ceylan C, Devrim Y. Green hydrogen based off-grid and on-grid hybrid energy systems. Int J Hydrogen Energy Dec. 2023;48(99):39084–96. https://doi.org/10.1016/j.ijhydene.2023.02.031.
[33] 'Energies | free full-text | estimating PV module performance over large geographical regions: the role of irradiance, air temperature, wind speed and solar spectrum'. https://www.mdpi.com/1996-1073/8/6/5159. [Accessed 29 January 2024].
[34] Lubitz WD. Effect of manual tilt adjustments on incident irradiance on fixed and tracking solar panels. Appl Energy May 2011;88(5):1710–9. https://doi.org/10.1016/j.apenergy.2010.11.008.
[35] Al-Quraan A, Al-Mahmodi M, Alzaareer K, El-Bayeh C, Eicker U. Minimizing the utilized area of PV systems by generating the optimal inter-row spacing factor. Sustainability Jan. 2022;14(10):10. https://doi.org/10.3390/su14106077.
[36] Dubey S, Sarvaiya JN, Seshadri B. Temperature dependent photovoltaic (PV) efficiency and its effect on PV production in the world – a review. Energy Proc Jan. 2013;33:311–21. https://doi.org/10.1016/j.egypro.2013.05.072.
[37] 'Pannelli fotovoltaici ad alta efficienza | Maxeon | SunPower Italia'. Accessed: January. 24, 2024.[Online]. Available: https://sunpower.maxeon.com/it/prodotti-pannelli-fotovoltaici/pannelli-fotovoltaici.
[38] Photovoltaic geographical information system (PVGIS) - European commission. https://joint-research-centre.ec.europa.eu/photovoltaic-geographical-information-system-pvgis_en. [Accessed 24 January 2024].
[39] Ayadi O, et al. Impacts of COVID-19 on educational buildings energy consumption: case study of the university of Jordan. Front. Built Environ. 2023;9(Jul). https://doi.org/10.3389/fbuil.2023.1212423.
[40] 'Energia. MiTE, firmato il Decreto che stabilisce nuovi limiti e orari per i riscaldamenti | Ministero dell'Ambiente e della Sicurezza Energetica' [Online]. Available: https://www.mase.gov.it/comunicati/energia-mite-firmato-il-decreto-che-stabilisce-nuovi-limiti-e-orari-i-riscaldamenti. [Accessed 29 July 2024].
[41] Ahmadi L, Fowler M, Young SB, Fraser RA, Gaffney B, Walker SB. Energy efficiency of Li-ion battery packs re-used in stationary power applications. Sustain Energy Technol Assessments Dec. 2014;8:9–17. https://doi.org/10.1016/j.seta.2014.06.006.
[42] Zuo H, Zhang B, Huang Z, Wei K, Zhu H, Tan J. Effect analysis on SOC values of the power lithium manganate battery during discharging process and its intelligent estimation. Energy Jan. 2022;238:121854. https://doi.org/10.1016/j.energy.2021.121854.
[43] Oji T, Zhou Y, Ci S, Kang F, Chen X, Liu X. Data-driven methods for battery SOH estimation: survey and a critical analysis. IEEE Access 2021;9:126903–16. https://doi.org/10.1109/ACCESS.2021.3111927.
[44] Kumar RR, Bharatiraja C, Udhayakumar K, Devakirubakaran S, Sekar KS, Mihet-Popa L. Advances in batteries, battery modeling, battery management system, battery thermal management, SOC, SOH, and charge/discharge characteristics in EV applications. IEEE Access 2023;11:105761–809. https://doi.org/10.1109/ACCESS.2023.3318121.
[45] Ah efficiency - an overview | ScienceDirect topics. https://www.sciencedirect.com/topics/engineering/ah-efficiency. [Accessed 2 July 2024].
[46] Boudghene Stambouli A, Traversa E. Fuel cells, an alternative to standard sources of energy. Renew Sustain Energy Rev Sep. 2002;6(3):295–304. https://doi.org/10.1016/S1364-0321(01)00015-6.
[47] K. Christian, 'The potential of hydrogen for decarbonising steel production'.
[48] Franco A, Giovannini C. Recent and future advances in water electrolysis for green hydrogen generation: critical analysis and perspectives. Sustainability Jan. 2023;15(24). https://doi.org/10.3390/su152416917. Art. no. 24.
[49] Small | McPhy. https://mcphy.com/it/apparecchiature-e-servizi/elettrolizzatori/small/. [Accessed 24 January 2024].
[50] Liponi A, Baccioli A, Ferrari L, Desideri U. Techno-economic analysis of hydrogen production from PV plants. E3S Web of Conferences Jan. 2022;334:01001. https://doi.org/10.1051/e3sconf/202233401001.
[51] 'HAUG. Sirius NanoLoc high pressure compressors: HAUG sauer kompressoren AG'. https://www.haug.ch/en/products-service/gas-compressors/haugsirius-nanoloc-11-30-kw.html. [Accessed 24 January 2024].
[52] Barbir F, Gómez T. Efficiency and economics of proton exchange membrane (PEM) fuel cells. Int J Hydrogen Energy Oct. 1997;22(10):1027–37. https://doi.org/10.1016/S0360-3199(96)00175-9.
[53] Kordesch K, Cifrain M. A comparison between the alkaline fuel cell (AFC) and the polymer electrolyte membrane (PEM) fuel cell. In: Vielstich W, Lamm A, Gasteiger HA, Yokokawa H, editors. Handbook of fuel Cells. 1. Wiley; 2010. https://doi.org/10.1002/9780470974001.f304065.
[54] Cleghorn SJC, et al. Pem fuel cells for transportation and stationary power generation applications. Int J Hydrogen Energy Dec. 1997;22(12):1137–44. https://doi.org/10.1016/S0360-3199(97)00016-5.
[55] Tatti R, Petrollese M, Lucariello M, Serra F, Cau G. Hydrogen storage integrated in off-grid power systems: a case study. Int J Hydrogen Energy Aug. 2024;79:164–76. https://doi.org/10.1016/j.ijhydene.2024.06.308.
[56] Choudhury A, Chandra H, Arora A. Application of solid oxide fuel cell technology for power generation—a review. Renew Sustain Energy Rev Apr. 2013;20:430–42. https://doi.org/10.1016/j.rser.2012.11.031.
[57] Fuel cell technology. https://www.ehgroup.ch/. [Accessed 24 January 2024].
[58] C. Isett, 'Calcolo Radiazione solare'. Università di Genova. [Online]. Available: https://architettura.unige.it/did/did1011/l2architettura5/quarto1011/imptec/matdid/cap10.pdf.
[59] Pradhan SK, Chakraborty B. Battery management strategies: an essential review for battery state of health monitoring techniques. J Energy Storage Jul. 2022;51:104427. https://doi.org/10.1016/j.est.2022.104427.